Vol 6 No 2 June 2025 Pages 30-43 e-ISSN 2708-5694

Journal of Agriculture, Food and Environment (JAFE)

Journal Homepage: https://journal.safebd.org/index.php/jafe

https://doi.org/10.47440/jafe.2025.6205

Research Article

OPEN ACCESS

Biosynthesis of Ag, Fe_2O_3, and hybrid Ag/Fe_2O_3 nanoparticles using clove (*Syzygium aromaticum*): A study on phytochemicals, antioxidant capacity, and antibacterial properties

El-Khateeb AY[1*], Alaa M[2], Amira E[2], Hager E[2], Heba W[2], Menna M[2], Menna Y[2], Nada G[2], Omnia A[2], Omnia M[2], Reem A[2], Elattar KM[3]

[1]Department of Agricultural Chemistry, Faculty of Agriculture, Mansoura University, Mansoura, 35516, Egypt.
[2]Department of Agricultural Biotechnology Program, Faculty of Agriculture, Mansoura University, Mansoura, 35516, Egypt.
[3]Unit of Genetic Engineering and Biotechnology, Faculty of Science, Mansoura University, Mansoura, 35516, Egypt.

Article History

Received: 03 April 2025

Accepted: 22 June 2025

Published: 30 June 2025

***Corresponding Author**

El-Khateeb AY (E-mail: aymanco@mans.edu.eg)

Keywords

Green synthesis, Silver nanoparticles, Iron oxide nanoparticles, Hybrid nanoparticles, Clove extract, Phytochemicals, Antioxidant activity, Antibacterial properties.

How to cite: El-Khateeb AY, Alaa M, Amira E, Hager E, Heba W, Menna M, Menna Y, Nada G, Omnia A, Omnia M, Reem A, Elattar KM 2025: Biosynthesis of Ag, Fe_2O_3, and hybrid Ag/Fe_2O_3 nanoparticles using clove (*Syzygium aromaticum*): A study on phytochemicals, antioxidant capacity, and antibacterial properties. J. Agric. Food Environ. 6(2): 30-43.

A B S T R A C T

In this work, the green synthesis of silver (Ag), iron oxide (Fe_2O_3), and Ag/Fe_2O_3 nanoparticles (NPs) was performed from the use of clove (*Syzygium aromaticum*) extract as a natural bioreducing and stabilizing agent. The rich content of clove extract by phytochemical components enables the successful transformation of metal ions into metal/metal oxide nanoparticles. The morphology characterization, functional groups, optical properties, and stability of the synthesized nanoparticles were investigated. The extract was recovered in part in the nanomaterials as revealed by phytochemical analysis, which detected phenolics (320.614 mg GAE/g), flavonoids (46.455 mg CE/g), and tannins (10.144 mg TAE/g). DPPH antioxidant activity showed strong radical scavenging capacity, showing an IC_{50} of 0.0098 from Ag/Fe_2O_3 NPs. This was almost equal to clove extract (0.0097 mg/mL) and far better than control ascorbic acid (0.0222 mg/mL). The antibacterial activity was found to be true against Gram-positive and Gram-negative bacteria. Ag/Fe_2O_3 NPs exhibited the widest spectrum and the greatest inhibition zones, largely against *S. aureus* (21±1.41 mm), *K. pneumoniae* (20±1.16 mm), and *S. typhimurium* (19±1.57 mm), as effective as or better than Azithromycin. The deposited results indicate that *S. aromaticum* is a potential *in situ* bioresource for multifaceted nanoparticle synthesis with high antioxidant and antimicrobial activity.

INTRODUCTION

Nanotechnology emerged in the last couple of decades as a revolutionary branch, presenting innovative solutions to countless fields, firstly in medicine, environmental science, and materials technology (Bayda *et al.*, 2019 & Kumar and Dixit, 2019). Of a great number of nanomaterial applications, nanoparticles of metals and metal oxides such as silver (Ag) and iron oxide (Fe_2O_3) have attracted close attention due to their particular physicochemical features and intensive biological activity (Idris and Roy, 2024 & Diabate *et al.*, 2023 & Mahmoud *et al.*, 2012). Silver nanoparticles are often described as having broad-spectrum antimicrobial activity, while iron oxide nanoparticles possess superior magnetic properties and biocompatibility, thus being usable in biomedical and environmental applications (Bamal *et al.*, 2021 & Naganthran *et al.*, 2022).

The traditional techniques of nanoparticle synthesis, while efficient, are also discovered to be centered on toxic chemicals, high energy demands, and environmentally unsafe by-products (Jain *et al.*, 2024). Owing to such

limitations, green synthesis methods have been intensely targeted as environmentally friendly alternatives (Ying *et al.*, 2022). All such green synthesis is usually carried out using the plant extracts, microorganisms, or other biomolecules as stabilizing and reducing agents (Vaseghi *et al.*, 2018). The plant-assisted synthesis is particularly used with many advantages such as simplicity, cost-effectiveness, scalability, and the inherent bioactivity of the phytochemicals that can enhance the functionality of the resultant end-product nanoparticles (Shah *et al.*, 2024b).

Syzygium aromaticum or clove is a spice and medicinally useful plant of general purpose with bioactive content as eugenol of high amounts, flavonoids, and phenolic acids (El-Saber Batiha *et al.*, 2020 & Haro-González *et al.*, 2021). The phytochemicals possess good reducing as well as antioxidant character and render clove a potential candidate for green synthesis of nanoparticles (Haiouani *et al.*, 2024). Clove extracts, as per previous research studies, have been documented to possess antimicrobial, antioxidant, and anti-inflammatory activities that are synergistic in nature when mixed and formulated as nanoparticles (Pandey *et al.*, 2024).

Green-synthesized Ag/Fe_2O_3 nanoparticles offer several opportunities in application development. Their antioxidant and antimicrobial properties make them suitable candidates for biomedical applications as wound dressings, antimicrobial coatings, and drug delivery agents (Sandhu *et al.*, 2024 & Ogwuegbu *et al.*, 2024). The imaging diagnosis, targeted therapy, and water purification functionalities are also enabled by the magnetism of Fe_2O_3 and the bactericidal capability of Ag. The plant-based synthesis also ensures environmental compatibility and scalability in industrial processes (Drishya *et al.*, 2025). Previously, *S. aromaticum* was described as a potent antioxidant, antimicrobial, and anti-inflammatory agent that owes its role to the eugenol content of the plant (El-Saber Batiha *et al.*, 2020). It has been investigated for silver nanoparticle biosynthesis; synthesis feasibility, biological activity. These studies, though, normally focus on a single case of nanoparticle and do not consider the use of clove extract to synthesize multifunctional hybrid systems such as Ag/Fe_2O_3. In this research, that gap is filled by integrating the phytochemical potential of clove with a hybrid nanoparticle design.

Notably, even though silver (Ag) and iron oxide (Fe_2O_3) nanoparticles have had wide-ranging use, it is worth noting that there is a massive gap in the literature when it comes to their coexistence, or hybrid states (Nishan *et al.*, 2023 & Shah *et al.*, 2024a). Synergism is often demonstrated in hybrid nanoparticles, culminating in possible upgraded functionality relative to monometallic analogues (Jiang and Xu, 2011). Little effort has been made with regard to the green synthesis of such hybrid entities using plant extracts. Especially, the possibility of the appearance of hybrid nanoparticles composed of Ag/Fe_2O_3 based on the extract from *S. aromaticum* (clove), which possess enhanced bioactivities, has not been studied extensively.

We herein report aqueous *S. aromaticum* clove extract-mediated biosynthesis of silver (Ag), iron oxide (Fe_2O_3), and Ag/Fe_2O_3 hybrid nanoparticles. The biosynthesized nanoparticles were characterized to analyze their morphological and physicochemical features. The extract was also subjected to phytochemical screening to understand its function in the nanoparticle formation. Antioxidant activity was documented by using standard assays, and antibacterial character of the nanoparticles was screened against certain Gram-negative and Gram-positive bacteria. In addition to demonstrating the green process in nanoparticle synthesis, this paper also hints at enhanced bioactivity of nanostructures of hybrid nature and thereby opens up avenues for their extensive future applications in biomedicine and antimicrobial technology.

MATERIALS AND METHODS

Reagents

The following chemicals were utilized in this study: Folin–Ciocalteu reagent (Fluka, Romania), gallic acid (Biomedical Inc., USA), and 1,1-diphenyl-2-picrylhydrazyl (DPPH$^{\bullet}$), aluminum chloride, sodium hydroxide, sodium nitrite, catechin hydrate, vanillin, sulfuric acid, hydrochloric acid, chitosan, and ascorbic acid, all obtained from Sigma-Aldrich (USA). Additional reagents included sodium carbonate and tannic acid, sourced from El-Nasr Pharmaceutical Chemicals (Egypt). Silver nitrate ($AgNO_3$) and ferric oxide (Fe_2O_3) were supplied by PIOCHEM for laboratory use.

Instruments

UV-Vis spectroscopy (Spekol 11, Analytik Jena AG, Jena, Germany) was employed to assess the optical properties of the samples. Functional groups were identified using FTIR spectroscopy (Thermo-Fisher Nicolet IS10, USA), at the Spectral Analyses Unit, Faculty of Science, Mansoura University, Mansoura, Egypt. High-resolution transmission electron microscopy (HR-TEM) was conducted using the Thermo Scientific Talos F200i using the carbon-coated grid (Type G 200, 3.05 µ diameter, TAAP, USA) to examine the morphology and structure of the nanoparticles. Zeta potential and particle size distribution analyses were carried out with a HORIBA Scientific SZ-100 "Ver 2.40" instrument at Egyptian Ministry of Defense, Egyptian Armed Forces, Chemical Warfare Department, Egypt. The plant extraction process was performed using a horizontal water bath shaker (Memmert WB14, Schwabach, Germany). Additionally, antioxidant and phytochemical assessments were conducted using a Spekol 11 spectrophotometer (Analytik Jena AG, Jena, Germany) at Genetic Engineering and Biotechnology Unit, Faculty of Science, Mansoura University, Mansoura, Egypt.

Preparation of the Clove Extract

Clove plant material was bought from a local market. 10 g of dried plant material was weighed and added to a 250 mL conical flask and mixed with 100 mL of 70% ethanol. The resulting mixture was shaken in a horizontal water bath shaker (Memmert WB14) at 250 rpm and 30 °C for 2 hours for improvement in extraction. The shake was kept overnight at room temperature to soak overnight after shaking to enhance the release of phytochemicals. The obtained extract was filtered with filter paper to remove solid residues and fresh used for nanoparticle synthesis and for biological, spectroscopic, and analytical studies (Ghoniem *et al.*, 2024 & Elattar *et al.*, 2025).

Green synthesis of nanocomposites

Synthesis of Ag and Fe_2O_3 NPs

The green synthesis of silver (Ag) and iron oxide (Fe_2O_3) nanoparticles was performed using aqueous extract of clove as both a reducing and stabilizing agent, based on previously established green synthesis procedures with slight modifications (Alanazi *et al.*, 2024 & Alanazi *et al.*, 2025 & Mert *et al.*, 2025). First, a 1 mM solution of silver nitrate ($AgNO_3$) was prepared by dissolving 50 mL of $AgNO_3$ in deionized water. Clove extract was prepared separately and diluted to a concentration of 4.85 mg/mL. To an agitated silver nitrate (200 mL) solution at room temperature, the clove extract (50 mL) was dosed dropwise. When the addition was complete, the reaction mixture was subjected to slow heating to 60 °C. A noticeable color transition from pale yellow to brown and from brown to dark brown served as an indication of silver nanoparticle formation. In order to prepare Fe_2O_3 nanoparticles, a 1 mM $Fe_2(SO_4)_3$ solution was prepared in deionized water. Clove extract was again added dropwise to 50 mL of this solution with the same stirring and heating. The reaction mixture was allowed to reach 60 °C for the mixture to turn into a reddish brown coloration, which gave evidence of iron oxide nanoparticles. In a case of hybrid nanoparticle synthesis, conditions were identical: equimolar solutions of silver nitrate and ferric sulfate were mixed and treated with clove extract. Immediately after synthesis, all nanoparticle suspensions were exposed to sonication at 80°C for 30 minutes to improve uniformity. The obtained colloids were centrifuged at 10,000 rpm for 10 minutes. The precipitated nanoparticles were harvested, cleaned three times with 70% ethanol to eliminate any remaining phytochemicals or non-reaction ions, and dried under 80 °C conditions to characterize them further in terms of spectroscopic and morphological studies.

Synthesis of Ag/Fe_2O_3 nanoparticles

Green synthesis of Ag/Fe_2O_3 nanoparticles was performed from aqueous clove extract as a reducing and stabilizing agent (Hammouda *et al.*, 2024). Two different, isolated equimolar (1 mM) aqueous solutions, silver nitrate ($AgNO_3$) and ferric sulfate ($Fe_2(SO_4)_3$), were developed in deionized water (50 mL each) separately. The two solutions were then mixed on a constant magnetic stirring to afford a homogeneous metal ion preceding solution. To the metal ion solution under stirring at room temperature was added dropwise an additional fresh solution of clove extract (50 mL, 4.85 mg/mL). After the extract had been added, the reaction mixture was heated slowly to 60°C and held at this temperature for 1 hour. During the formed reaction, there was slow color changing: from pale yellow to reddish brown and then to dark brown, which implies the formation of silver and iron oxide nanoparticles as well as their possible hybridization. In order to ensure uniform dispersion and interaction of the metal nanoparticles, the reaction was done in ultra-sonication for half an hour at 80°C. The resulting hybrid nanoparticle suspension was centrifuged for 10 minutes at 10,000 rpm to induce the separation of the solid product. The resulting precipitate was washed repeatedly using 70% ethanol until any free phytochemicals or unreacted ions were removed. The product was dried at 80°C and stored for further characterization.

Phytochemical Analysis

Tannin content was determined through the use of the well-established vanillin-hydrochloride technique as described in findings of past studies (Elattar *et al.*, 2024a). The method comprises the reaction between the sample and a freshly prepared vanillin-hydrochloride reagent, leading to the color change, quantified as absorbance at 500 nm. The curves of a standard tannic acid were used to approximate the content os tannins using Y = 0.0009X and R^2 = 0.955. Total phenolic content (TPC) of the samples was also measured by using the Folin-Ciocalteu method as described previously (Sánchez-Rangel *et al.*, 2013 & Elattar *et al.*, 2023). The results were expressed as mg GAE / sample, based on a gallic acid calibration curve (y = 0.0062x) and R^2 = 0.987. Flavonoid content was determined by using a colorimetric assay, with aluminum chloride as the complexing agent. Using previously described methods, flavonoid amount was extrapolated based on a standard quercetin curve, y = 0.0028x, with an R^2 = 0.988 (Shraim *et al.*, 2021).

Antioxidant activity

DPPH$^{\bullet}$ assay (Elattar *et al.*, 2024b) was utilized for estimation of antioxidant activity of samples, taking reference standard as ascorbic acid. An equal volume of serial dilution of the sample was added to a freshly prepared solution containing 0.135 mM DPPH$^{\bullet}$ methanol and kept at room temperature in the dark for 30 minutes. Absorbance at 517 nm was noted, and the percentage of DPPH$^{\bullet}$ remaining radicals was estimated from (Eq. 1):

$$\%DPPH^{\bullet}\ remaining = [DPPH^{\bullet}]_T / [DPPH\cdot]_{T=0} \times 100 \rightarrow (Eq.\ 1)$$

where $[DPPH^{\bullet}]_T$ is the absorbance at time *T*, $[DPPH^{\bullet}]_{T=0}$ is the control sample absorbance (equal volume of DPPH and methanol without the tested sample). IC_{50}, the 50% inhibition concentration for DPPH$^{\bullet}$ radicals, was obtained from the curve of residual DPPH$^{\bullet}$ against sample concentration by exponential regression. The lower IC_{50} values indicate higher antioxidant activity.

Antibacterial Assessments

The antibacterial property of the test samples was examined using the agar well diffusion method (Eldadamony *et al.*, 2024 & Ghoniem *et al.*, 2024). Mueller-Hinton agar plates were inoculated by spreading the bacterial suspension over the plate evenly. Wells (6 mm diameter, 5 mm depth) were created aseptically with the help of a sterile cork borer, and 100 µL of every sample was filled into the wells. Azithromycin was employed as a positive control to validate the assay. Plates were incubated at 37°C for 24 hours to promote the growth of bacteria and interaction with the test substance. Zones of inhibition, colorless areas surrounding the wells in which the bacteria failed to grow, were observed after incubation. Larger zones of inhibition were indicative of high antibacterial activity. The method relies on the diffusion of the antimicrobial compounds within the agar medium, where they have an inhibitory effect on target microbial species.

Statistical process and software

Statistical analysis was conducted using SPSS software version 21. Results from experimental results were shown as mean ± standard deviation (SD) for triplicate measurements. A p-value ≤ 0.05 was employed for comparison between groups.

RESULTS AND DISCUSSION

UV-Visible Spectroscopy

The UV-Vis spectroscopy analysis was carried out to confirm the synthesis and optical properties of the prepared nanoparticles. The recorded absorbance and corresponding wavelengths for each sample are presented in the table above. To assess the synthesis of the nanoparticles and test their optical response, UV-Vis spectroscopy was employed. In Figure 1, there are the absorbance values and their corresponding wavelength of every sample obtained from the absorbance spectra. The absorbance values of the presence of clove extract, both as the reducing and stabilizing agent, were found to be at the wavelengths of 474.0 nm and 1.041. This is because the extract contains polyphenolic and other phytochemical compounds that are known to be involved in metal ion reduction and stabilization of nanoparticles. The SPR peak was found at 513.0 nm, and the absorbance was 1.277 for the synthesized Ag NPs, which were quite sharp and strong. This peak supports the formation of Ag NPs because it was in the observing range of SPR (400-550 nm), typically for the silver nanoparticles. The increase in absorbance, relatively, translates to a high concentration of the nanoparticle in solution. Fe_2O_3 NPs showed a broader and higher peak at 571.0 nm having absorbance value of 1.238. This shift to the red region in the wavelength relative to Ag NPs by Fe_2O_3 NPs can be attributed to the optical characteristics of the Fe_2O_3 NPs, as supported by earlier literature (Kumar *et al.*, 2022 & Mohan *et al.*, 2022). The peak position corresponds to iron oxide nanoparticles, confirming that they were synthesized effectively. The bimetallic Ag/Fe_2O_3 NPs had an absorbance peak at 516.0 nm with a lesser absorbance value of 0.799. The slight red shift of pristine Ag NPs indicates some interaction between silver and iron oxide constituents with the bimetal system (Padilla-Cruz *et al.*, 2021). The reduction in absorbance may indicate a dilute concentration or altered particle size and morphology due to being in the bimetal form (Wang *et al.*, 2005). The shift, along with intensity change, further supports in favor of successful formation of Ag/Fe_2O_3 NPs.

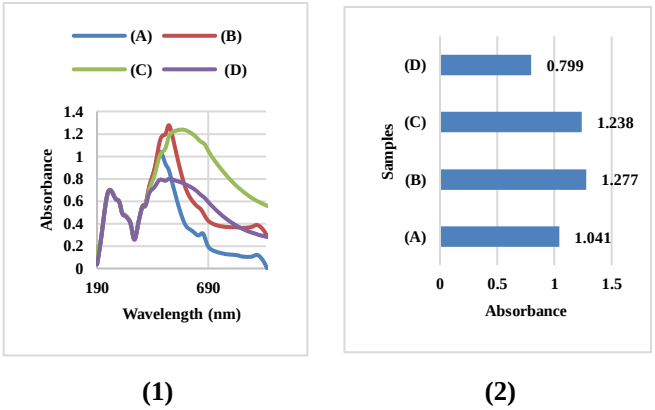

(1) **(2)**

Figure 1. UV-visible spectroscopic results. (1) The sample absorbance was recorded at varied wavelengths (nm). (2) A comparison of the maximum absorbance recorded at the higher wavelengths (nm). (A) Clove extract; (B) Ag NPs; (C) Fe_2O_3 NPs; and (D) Ag/Fe_2O_3 NPs.

Table 1: Electronic Transitions of the clove extract and nanomaterials

Sample	Observed Transition Type	Description
Clove extract	π→π*, n→π*	Organic chromophores from phytochemicals
Ag NPs	Surface Plasmon Resonance	Collective oscillation of conduction electrons
Fe_2O_3 NPs	LMCT, d-d transitions	Electron transfer between ligands and Fe^{3+} centers
Ag/ Fe_2O_3 NPs	Hybrid SPR + LMCT	Combined effects of Ag plasmonics and Fe charge transfer

In general, the UV-Vis spectrum analysis also shows the existence of single and bimetallic nanoparticles, and the peaks of dip and peak correspond to their nature. These variations are suggestive of the optical characteristics and interspecific communication of the metallic parts in bimetallic nanoparticles. The peak absorbance of the clove extract occurred at 474.0 nm with an intensity of 1.041 and is attributed to the existence of polyphenolic compounds and other phytochemicals that can exhibit π→π* and n→π* electronic transitions (Table 1). The usual transformations of the conjugated and aromatic systems also support the existence of the bioactive molecules, which can decrease metal ions and solidify the subsequent nanoparticles (El-Seedi *et al.*, 2019). Among the prepared Ag NPs, the sample had a SPR at 513.0 nm with the maximum absorbance value of 1.277. This is because conduction band electrons in metallic nanoparticles can coherently oscillate the incoming light, a feature unique to plasmon resonance (Halas *et al.*, 2011). This is not a typical molecular transition but a result of the oscillation of electrons in the form of dipolar plasmon resonance, which is a sign of synthesized and stable Ag NPs. The Fe_2O_3 NPs, on the other hand, showed a broader peak at 571.0 nm and an absorbance of 1.238 due to Metal to Ligand and Ligand to Metal Charge Transfer (LMCT) and d-d transitions in the Fe^{3+} centers of the nanoparticles (Kumar *et al.*, 2023).

These shifts can be attributed to the changes which are typical of transition metal oxides and reflect the more prone to change electronic structure of iron-based nanomaterials. The samples with Ag/Fe_2O_3 NPs had the highest peak at 516.0 nm, the coulometer and reduced absorbance at 0.799 for the periodic table due to the electronic interaction of Ag and Fe_2O_3. This slight red shift of the SPR peak of the Ag NPs implies that there could be electronic coupling between the metallic and oxide phases that alters the plasmonic properties (Khurana and Jaggi, 2021). The decrease in absorbance might indicate a decrease in the particle concentration, or changes in sample morphology, or SPR, where the iron oxide matrix may have caused partial damping. Ideally, the bimetallic system would show a combination of both the SPR and charge transfer transitions, thus providing evidence that there was successful formation of unique composite nanoparticles.

FTIR Spectroscopy

Fourier Transform Infrared (FTIR) spectroscopy was employed to identify functional groups in clove extract and

nanoparticles synthesized (Figure 2 & Table 2). Spectral information indicates the nature of phytochemicals involved in nanomaterial synthesis and surface chemistry of resultant nanomaterials. The strongest absorption bands of clove extract were at 3383 cm^{-1} and are due to O-H stretching vibrations of phenol and alcohol, indicating strong hydrogen bonding. Bands at 2918 and 2848 cm^{-1} are due to C-H stretching vibrational modes of aliphatic chains. The two vibrations at 1723 and 1706 cm^{-1}, which are given off by the carbonyl groups (C=O), are typical of aldehydes, ketones, or carboxylic acids. Similar results were also observed by (Shahriary *et al.*, 2018), in which bands of O-H and C=O stretching of *Stachys lavandulifolia* extract supported the formation of Ag nanoparticles. The bands observed at 1656, 1613, and 1587 cm^{-1} can be attributed to C=C stretching in the aromatic rings, while bands observed at 1512 cm^{-1} and 1446 cm^{-1} can perhaps be assigned to aromatic skeletal motion. Phenolic and ether groups C-O, C-N, and other bent modes of 1347, 1181, 1104, 1076, 1035, and 1008 cm^{-1} bands are due to the profuse presence of bioactives.

Some bands of the clove extract were also found within the FTIR spectrum of Ag NPs and include the O-H stretching band at 3373 cm^{-1} and the C=O stretching at 1724 cm^{-1}; these reveal the fact that these functional groups play a major role in the reduction and capping of the nanoparticles. The two sharp bands at 1656 and 1611 cm^{-1} are due to the C=C of the aromatic ring, and the bands at 1512, 1448, and 1374 cm^{-1} are convincing evidence of phenolic compounds adsorbed on the surface of the nanoparticle. The new or increased bands at 640, 597, and 519 cm^{-1} were assigned to metal of metal-oxygen (Ag-O) stretching, and these prove that the synthesis of Ag NPs in the presence of organic capping layers has been successful. Similar results were also obtained by (Deshmukh *et al.*, 2019), in which Ag NPs synthesized using fenugreek seed extract consisted of Ag-O stretching bands, indicating successful formation of nanoparticles.

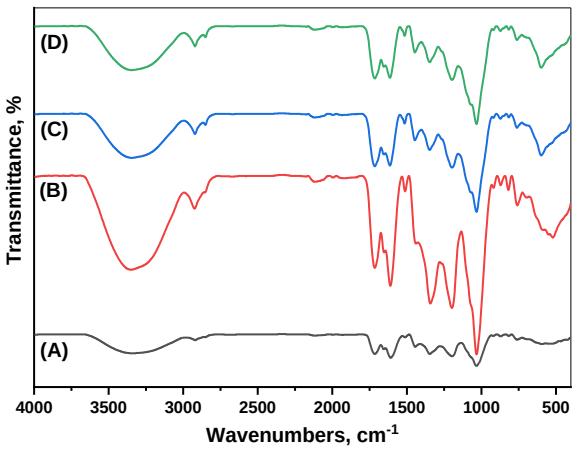

Figure 2. FTIR spectral charts of clove extract and synthesized nanoparticles. (A) refers to clove extract; (B) refers to Ag NPs; (C) refers to Fe_2O_3 NPs; (D) refers to Ag/Fe_2O_3 NPs.

In the spectrum of Fe_2O_3 NPs, the peaks observed include 3361, 2919, and 2850 cm^{-1} for the clove extract with residue. Selective peaks at 1727, 1713, and 1690 cm^{-1} suggest its high reactivity with carbonyl groups. Other bands, such as the aromatic and C=C stretching vibrations, are present at 1657, 1610, and 1514 cm^{-1}. Especially, the bands at 602 cm-1 and their nearby regions can indicate Fe-O stretching typical of iron oxide due to the formation of nanoparticles. (Mirza *et al.*, 2018) observed similar results in their investigation on *Agrewia optiva* and *Prunus persica* extracts, where the Fe-O stretching bands confirmed the iron oxide nanoparticle formation.

Table 2: FTIR spectral interpretation of clove extract and synthesized nanoparticles

Sample	Wavenumber (cm^{-1})	Characteristic Group	Interpretation
Clove Extract	3383	O-H stretching (phenols)	Hydrogen bonding, polyphenolic compounds aiding in reduction
	2918, 2848	C-H stretching (alkanes)	Aliphatic chains from organic compounds
	1723, 1706	C=O stretching (carbonyls)	Aldehydes/carboxylic acids; involved in reduction
	1656-1587	C=C stretching (aromatics)	Aromatic structures confirming the presence of bioactive compounds
	1512-1446	C-C/C-H bending (aromatics)	Skeletal vibrations from substituted aromatics
	1347	O-H bending	Phenols: possible involvement in capping
	1181-1008	C-O, C-N stretching	Alcohols/ethers contributing to nanoparticle stabilization
	918-764	=C-H out-of-plane bending	Aromatic substitutions
Ag NPs	3373	O-H stretching	Retained from clove extract; capping agent
	2921	C–H stretching	Organic capping layer
	1724, 1656	C=O stretching	Organic compounds coordinated to the Ag surface
	1611, 1512	C=C stretching	Aromatic rings from the extract
	1374-1009	C-N, C-O stretching	Functional groups involved in stabilization
	640, 597, 519	Ag-O stretching	Formation of Ag nanoparticles confirmed
Fe_2O_3 NPs	3361	O-H stretching	Surface hydroxyl groups or residual phytochemicals
	2919, 2850	C-H stretching	Organic stabilizers
	1727-1690	C=O stretching	Organic components; involved in Fe ion reduction
	1657-1514	C=C stretching	Aromatic functional groups
	1348-1031	C-O, C-N stretching	Surface-bound phytochemicals
	872, 816, 763, 602	Fe-O stretching	Confirmation of iron oxide formation
Ag/ Fe_2O_3 NPs	3351	O-H stretching	Phytochemical residues acting as capping agents
	2920, 2849	C-H stretching	Aliphatic hydrocarbon groups
	1724, 1692	C=O stretching	Organic molecules involved in dual metal coordination
	1656-1512	C=C stretching	Aromatic systems contributing to stabilization
	1349-1036	C-O, C-N stretching	Bonding of phytochemicals to the surface
	916, 874, 818, 764	Aromatic out-of-plane bending	Indicate the structural integrity of plant-based compounds
	601, 522	Fe-O, Ag-O stretching	Confirm hybrid nanoparticle formation

The spectrum of bimetallic Ag/Fe_2O_3 NPs contained the peaks from Ag and Fe_2O_3 NPs. In the spectra, the O-H stretching vibrations were observed at 3351, 2920, and 2849 cm^{-1}, while C=O stretching vibrations were observed at 1724 and 1692 cm^{-1}. Phytochemical constituents remained stable, with C=C aromatic vibrations remaining as 1656, 1612, and 1512 cm^{-1}. Remarkably, metal-oxygen vibrations were seen at 601 and 522 cm^{-1}, suggesting the presence of Ag-O and Fe-O bonds. (Cakić *et al.*, 2018) reported similar results in their study on silver nanoparticles prepared from *Fumaria officinalis* extract, where FTIR analysis confirmed the presence of metal-oxygen bonds and phytochemical capping.

The overlap and retention of functional group bands of clove extract suggest successful stabilization of the bimetallic nanoparticles through the adsorption of phytochemicals. These FTIR findings overall confirm that clove extract phytochemicals, in the predominant phenols, carbonyls, and aromatics, play key roles in capping and bioreducing metal ions to form Ag, Fe_2O_3, and Ag/Fe_2O_3 nanoparticles. The presence of metal-oxygen stretching vibrations in the fingerprint zone (less than 700 cm^{-1}) is a concrete indication of nanoparticle synthesis and surface functionalization through bio-organic molecules. In summary, FTIR analysis confirms that phytochemicals in the clove extract, such as phenolic components and carbonyl groups, are the agents reducing and stabilizing Ag, Fe_2O_3, and Ag/Fe_2O_3 nanoparticles. The functional groups and metal-oxygen vibrations identified are consistent with the literature, and this confirms the effectiveness of plant extracts as facilitators of green nanoparticle synthesis.

Zeta Potential and DLS Analysis

Colloidal stability and surface charge of the nanoparticles that were generated were tested through zeta potential measurement. Zeta potential is a crucial parameter in which electrostatic attraction or repulsion among particles that are suspended in solution can be anticipated, as well as whether a dispersion is stable (Figure 3). A mean zeta potential value of -2.5 mV was registered in Ag NPs, indicative of low surface charge and ineffective electrostatic repulsion between the particles. The zeta potential of -0.000019 $cm^2/V{\cdot}s$ and conductivity of 6.479 mS/cm were the same. Low zeta potential value suggests that Ag NPs can possibly coagulate with time, and their relatively higher conductivity suggests metallic nature and higher ionic character of the colloidal solution.

Conversely, the iron oxide nanoparticles (Fe_2O_3 NPs) possessed a more negative zeta potential of -9.1 mV, electrophoretic mobility of -0.000071 $cm^2/V{\cdot}s$, and conductivity of 1.133 mS/cm. The greater negative zeta potential than Ag NPs indicates greater electrostatic stabilization, which can result in better dispersion and reduced aggregation (Badawy *et al.*, 2010 & El Badawy *et al.*, 2012). This is in accordance with the semiconducting nature of iron oxide as well as the fact that there are fewer free ions within the medium.

The bimetallic Ag/Fe_2O_3 nanoparticles showed a zeta potential between intermediate with a value of -7.4 mV, meaning there is intermediate colloidal stability as per the mixed surface properties of the constituents. Electrophoretic mobility was -0.000058 cm^2/Vs, while conductivity was 1.254 mS/cm. The values suggest a balancing interaction between the Ag and Fe_2O_3 phases such that the silver makes contributions to enhanced ionic conductivity, and the iron oxide makes contributions to enhanced surface charge stabilization (Kumar *et al.*, 2022). Generally, while no nanoparticles have zeta potentials in the high stability range (±30 mV or higher) (Tantra *et al.*, 2010), both the Fe_2O_3 and the Ag/Fe_2O_3 NPs demonstrate enhanced electrostatic stabilization compared to Ag NPs alone. The measurements of zeta potential also indicate the contribution of compositional engineering to determining the quality of the surface charge and colloid behavior of the nanoparticles.

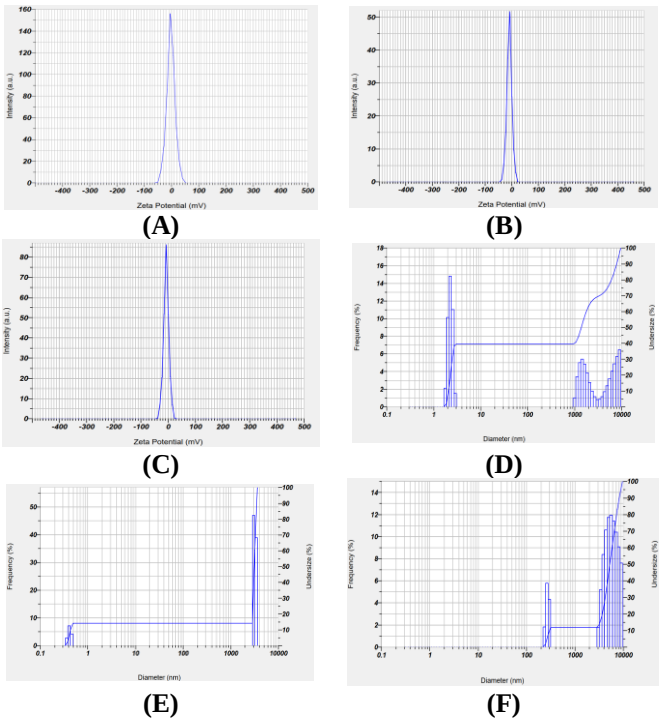

Figure 3. Zeta potential and DLS analysis of the nanoparticles. (A) Zeta potential analysis of Ag NPs. (B) Zeta potential analysis of Fe_2O_3 NPs. (C) Zeta potential analysis of Ag/Fe_2O_3 NPs. (D) DLS analysis of Ag NPs. (E) DLS analysis of Fe_2O_3 NPs. (F) DLS analysis of Ag/Fe_2O_3 NPs.

Dynamic Light Scattering (DLS) was conducted to determine the hydrodynamic size distribution and polydispersity of the resulting nanoparticles. Zeta average (or hydrodynamic diameter) provides information on the effective size of suspended particles, while the polydispersity index (PDI) provides information on the homogeneity of particle size distribution. The lower the PDI value (preferably <0.3), the more monodisperse the system; values >0.3 report growing size heterogeneity. The DLS measurements showed the silver nanoparticles (Ag NPs) had a zeta average of 2113.5 nm and a PDI of 0.489, exhibiting a very wide size distribution and significant polydispersity. The gigantic hydrodynamic diameter is very likely to be the result of nanoparticle aggregation in suspension, as was indeed discovered in accordance with the low zeta potential (-2.5 mV) from the earlier measurements, validating poor electrostatic stabilization. Iron oxide nanoparticles (Fe_2O_3 NPs) also exhibited an even larger hydrodynamic diameter of 2743.0 nm with a likewise lower PDI of 0.408, again indicative of polydisperse behavior. Though they had a more negative zeta potential (-9.1 mV), the Fe_2O_3 NPs also easily aggregated, presumably due to magnetic particle-particle interactions typical in iron oxide systems. The Ag/Fe_2O_3 bimetallic nanoparticles had the largest hydrodynamic diameter of 3114.4 nm and a PDI of 0.485, which is similar in polydispersity to that of Ag NPs. The increased particle

size may be due to the combined effect of metal-metal interaction and the presence of relatively less stable, larger aggregates due to the inadequate surface passivation (Zhang *et al.*, 2010 & Cartwright *et al.*, 2020). Generally, the DLS data reveal that all samples exhibit significant polydispersity and aggregation when in aqueous environments, particularly the bimetallic system. The findings underscore the need for more effective stabilization processes to achieve narrower size distributions and enhanced dispersion stability.

High Resolution-Transmission Electron Microscopy (HR-TEM)

It was used for studying the morphology, size, and dispersibility of the biosynthesized silver nanoparticles by HR-TEM. From the HR-TEM micrograph (Figure 4a), it was noted that the Ag NPs were mostly spherical in shape, with relatively homogeneous formatting in the observed field. The nanoparticles were well dispersed, but there was agglomeration in some areas, as it is common for the biologically synthesized nanoparticles since organic capping agents from the plant extract are apt to be adsorbed onto the Ag NPs. The size of Ag NPs was estimated to be 10-50 nm, and it was consistent with the provided scale bar of 50 nm. Such sizes at the nanoscale attest to the successful reduction and stabilization of silver ions of clove extract's bioactive constituents. Particle smooth surfaces and clearly defined boundaries also suggested their high purity and crystallinity. The green synthesis process with the use of clove extract was likely to be used in particle size control and preventing uncontrolled growth, in which the secondary metabolites: eugenol, flavonoids, and tannins act as reducing and capping agents (Elbagory *et al.*, 2022 & Karaman and Kaplan, 2022). These molecules are adsorbed on the surfaces of the nanoparticle and stabilize the nanoparticle and preventing agglomeration. Generally, the HR-TEM analysis validated the green synthesis of nanosized, spherical Ag NPs that can be applied to biomedical and varied types of antimicrobial applications.

Biosynthesized Fe_2O_3 nanoparticles' structural and morphological properties were also studied using HR-TEM (Figure 4b). The Fe_2O_3 NPs showed irregular morphologies, from semi-spherical to polygonal in shape, with a tendency towards dense aggregates or clusters. Such aggregation can be explained by the magnetic properties of Fe_2O_3, causing strong inter-particle magnetic interactions. It may also be due to partial stabilization by the phytochemicals of the used clove extract during synthesis. Particle size in the range of 10-30 nm was noted, as concluded from the 200 nm scale bar. Despite being closely packed, nanoparticle boundaries were clear for individual nanoparticles, which indicates that aggregation was physical and not through complete fusion (Shrestha *et al.*, 2020). The contrast and resolution of the image showed that the Fe_2O_3 nanoparticles possessed superior crystallinity. Green synthesis using clove extract provided both reducing and capping functionality, and the phytochemicals, like polyphenols and flavonoids, were accountable for nanoparticle formation. However, the relatively high magnetic interaction among Fe_2O_3 particles may have limited the stabilizing action of these phytochemicals to cause partial aggregation (Nandhini and Shobana, 2023). Nevertheless, HR-TEM characterization was utilized to confirm successful biosynthesis of crystalline nanoscale Fe_2O_3 particles with suitable properties for antibacterial, catalytic, and magnetically responsive biomedical applications (El-Khateeb *et al.*, 2025).

The morphological architecture of the biosynthesized Ag/Fe_2O_3 nanocomposite was analyzed by HR-TEM imaging (Figure 4c). The micrograph revealed a heterogeneous network of nanoparticles typical of a properly organized composite structure that encompassed silver (Ag) and iron oxide (Fe_2O_3) nanoparticles. Significantly, the TEM image revealed dark contrast regions, which were typical of electron-rich Ag NPs, dispersed within a light, diffused Fe_2O_3 matrix. The Ag NPs preserved their spherical shape and were mostly observed anchored on or embedded within the irregular Fe_2O_3 network, which exhibited a porous and aggregated texture. The particle size of the composite was 10-40 nm, thereby affirming that both materials were still in the nanoscale following the co-synthesis. This incorporation into the structure suggests a synergistic interaction between Ag and Fe_2O_3 that could result in enhanced functional properties. *S. aromaticum* extract facilitated the co-synthesis of metals and provided phytochemicals that could reduce as well as stabilize both the metal precursors at the same time (Sharma *et al.*, 2022). Homogeneous distribution and surface interaction between Ag and Fe_2O_3 are most probably the reasons behind the improvement in reported antibacterial activity, as seen in biological assays. This would be a result of the synergistic antimicrobial effect of Ag and the ROS-generation capability of Fe_2O_3. Generally, HR-TEM analysis confirmed successful biosynthesis of a highly dispersed, crystalline Ag/Fe_2O_3 nanocomposite, whose structural features are most favorable for multifunctional biomedical applications, particularly those requiring synergistic antimicrobial activity.

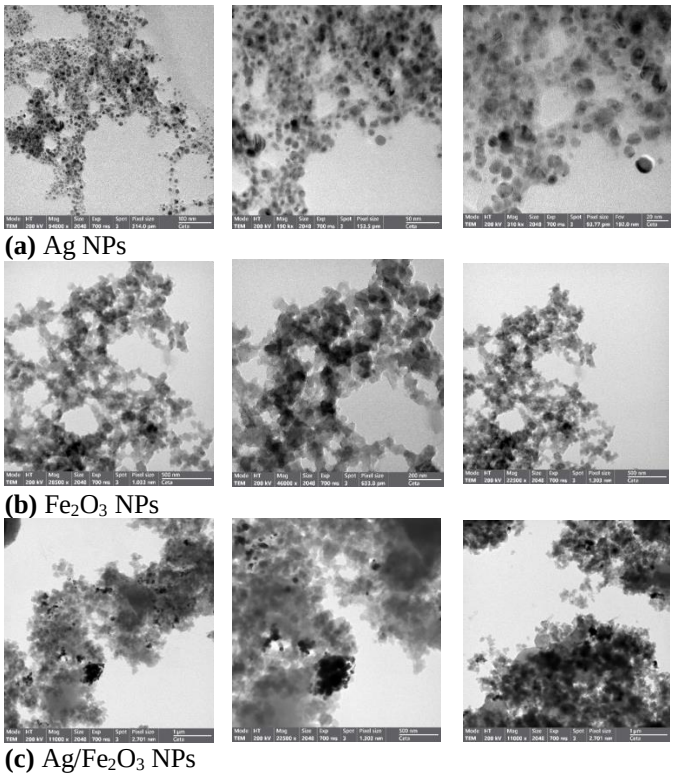

(a) Ag NPs

(b) Fe_2O_3 NPs

(c) Ag/Fe_2O_3 NPs

Figure 4. HR-TEM micrographs of nanomaterials.

Phytochemical Analysis

Phytochemical, phenolics, flavonoids, and tannins were quantitatively established for clove extract and green-synthesized nanoparticles, findings of which were summarized in Figure 5. Phenolics were maximum in the clove extract (320.614 mg GAE/g) thus validating its proud

polyphenolic content. During the nanoparticle synthesis, the total phenolic content reduced in all nanomaterial formulations, indicating their active participation in reduction and stabilization reactions in green synthesis. Among the nanoparticles studied, the Ag/Fe_2O_3 NPs contained the highest phenolic content, 244.592 mg GAE/g, followed by Ag NPs (194.113 mg GAE/g) and reflect greater preservation or improved capping capability in the bimetallic system. The same trend was observed in the case of flavonoid content, the value was highest for clove extract (46.455 mg CE/g), and Ag/Fe_2O_3 NPs had also a relatively higher flavonoid content (36.321 mg CE/g) when compared with monometallic nanoparticles. This suggests that flavonoids were actively involved in nanoparticle formation and can in part be fixed on nanoparticle surfaces. The highest level of tannin was found on clove extract (10.144 mg TAE/g) and all the contents of nanoparticles were lower. The Ag/Fe_2O_3 again had the highest of the nanomaterials (5.573 mg TAE/g), which means higher retention or a stronger interaction with the tannin molecules. The general lowering of phytochemical content after nanoparticle synthesis confirms their tremendous effectiveness as natural reducing and stabilizing agents for biosynthesis processes. The better retention of the bioactive compounds in the bimetallic Ag/Fe_2O_3 NPs demonstrates a synergistic interaction which might improve their biological functionality.

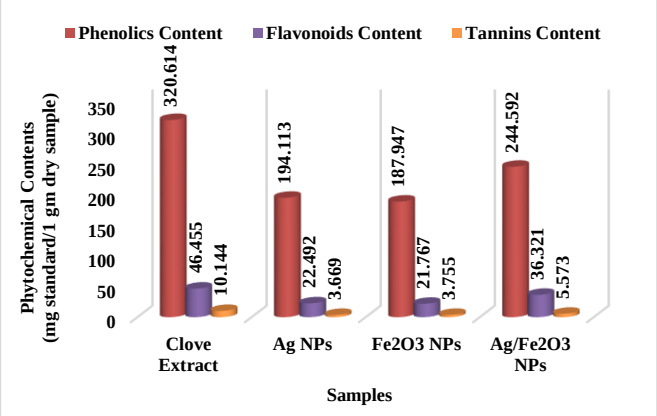

Figure 5. The results of phytochemical analysis.

The noted decline in the phenolics, flavonoids, and tannins in the synthesized nanomaterials in comparison to the crude clove extract may be traced through the active participation of these phytochemicals in the bioreduction and stabilization processes during the synthesis of the green nanoparticle (Park *et al.*, 2011 & Ovais *et al.*, 2018). Phenolic and flavonoid compounds, which are also known to have electron-donating capacity, have an important role to play in the reduction of metal ions (e.g., Ag^+, Fe^{3+}) to their respective nanoparticles [Ag^0, Fe_2O_3]. In this redox procedure, the phytochemicals are oxidized, resulting in a quantifiable reduction of their number in the created nanomaterial. In addition, most of these bioactive molecular species adhere to the nanoparticle's surface as natural caps that stabilize and prevent aggregate activity. This surface adsorption further reduces their detectable content in post-synthesis extracts. Phytochemical retention in the bimetallic Ag/Fe_2O_3 NPs, relatively more, could suggest that they may either have higher encapsulation efficiency or no consumption of reducing agents in the synthesis, likely because of synergistic redox kinetics between the two metals. Our results are in line with the previous studies that specified the significant role of phytochemical molecules in the transformation of metal ions into metal/metal oxide nanoparticles (Alanazi *et al.*, 2024 & Elattar *et al.*, 2025).

Antioxidant Activity

Antioxidant properties of the obtained nanomaterials and clove extract were investigated through the DPPH$^{\bullet}$ assay with ascorbic acid as a standard. The % DPPH$^{\bullet}$ radical scavenging and % of IC_{50} in presented in Figures 6 and **7**, respectively. The antioxidant activity of the clove extract was high (IC_{50} value was 0.0097 mg/mL, which is almost equal to Ag/Fe_2O_3-nanocomposite 0.0098 mg/mL) and lower than the standard ascorbic acid (0.0222mg/mL). This high level of antioxidant activity can be attributed to the high level of polyphenols and flavonoids in the extract, which is expounded above. Silver/iron oxide (Ag/Fe_2O_3 NPs) displayed the highest scavenging activity amongst prepared nanomaterials and was very close to the scavenging activity of clove extract, thereby suggesting synergistic antioxidant activity in the silver/iron oxide components. This suggests combined efforts that augment the electron-donating capability for both metals, possibly due to increased surface area and increased availability of active sites. Fe_2O_3 NPs were found to exhibit good antioxidant activity (IC_{50} = 0.0182 mg/mL), stronger than that of Ag NPs (IC_{50} = 0.0418 mg/mL), which can be attributed to the redox-active nature of iron oxide and to DPPH radical interaction. Scavenging activity of all nanomaterials was surprisingly found to rise with rising concentration, hence confirming concentration-dependent antioxidant activity. By comparing IC_{50} values of nanomaterials with the raw extract, a reduction in IC_{50} values of nanomaterials verifies that phytochemicals involved in capping nanoparticles are responsible for retained or enhanced antioxidant activity. The outcomes also reveal that close extraction induced green synthesis not only allows one to synthesize nanoparticles but also retains antioxidant potential, especially bimetallic Ag/Fe_2O_3 systems. This suggests their potential viability for biomedical and pharmaceutical applications in which modulation of oxidative stress is essential.

The antioxidant activity of the synthesized nanomaterials, especially the Ag/Fe_2O_3 nanocomposite, can be mainly attributed to its electron or hydrogen releasing power, for the neutralization of free radicals such as DPPH$^{\bullet}$.

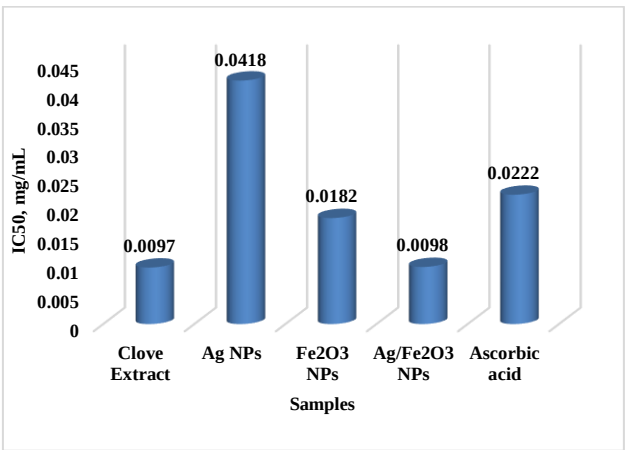

Figure 6. Comparison of the antioxidant results expressed as IC_{50} in mg/mL of the water extracts relative to the antioxidant standard.

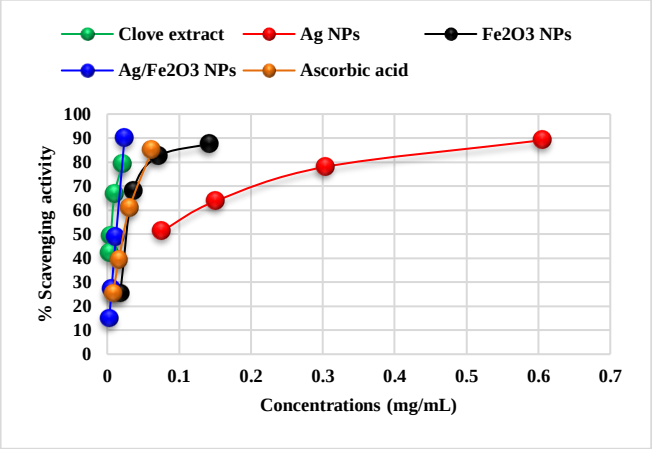

Figure 7. The results of antioxidant activity plotted the % scavenging activity versus the sample concentration.

Under DPPH assay conditions, radicals receive electrons from antioxidant molecules, causing a reduction in the absorbance at 517 nm that can be measured quantitatively. As far as green-synthesized nanoparticles are concerned, bioactive phytochemicals in the clove extract, i.e., polyphenols and Flavonoids, are attached to the surfaces of the molecules during the process of synthesis (El-Maati *et al*., 2016 & Saeed *et al*., 2021 & Haiouani *et al*., 2024) and have two roles: metal ion reduction and capping of the nanoparticles (Sharma *et al*., 2020). The phytochemicals bound to the surface remain redox active, having functional groups that involve radical scavenging (Seyoum *et al*., 2006). In addition, the presence of silver and iron oxide in the bimetallic Ag/Fe_2O_3 nanocomposites increases this activity through a synergistic effect; it is due to the provision of more surface area, better charge transfer, and enhanced reactivity towards electron-deficient radical species. The outcome is an effective antioxidant system that is able to scavenge free radicals successfully, as supported by the low IC_{50} values noted.

Antibacterial activity

Antibacterial activity of clove extract, biosynthesized Ag and Fe_2O_3 NPs, and Ag/Fe_2O_3 NC was tested against a panel of Gram-positive and Gram-negative pathogenic bacteria using the agar well diffusion method. Inhibition zones (mm) are presented in Table 3 & Figure 8. The results showed variation in antibacterial activity between the test samples. *Escherichia coli* was relatively susceptible to all treatments, and Ag NPs produced the biggest inhibition zone (17±1.08 mm), which was comparable with azithromycin (17 ± 1.22 mm). Clove extract alone was active (14±1.50 mm), suggesting the presence of bioactive phytochemicals possessing antimicrobial properties. *Salmonella typhimurium* was most sensitive to the Ag/Fe_2O_3 NC (19 ± 1.57 mm), being more than individual Ag (13 ± 1.09 mm) and Fe_2O_3 NPs (no inhibition), which suggests a synergistic effect in the nanocomposite. There were no data for azithromycin or DMSO controls for this strain. *Klebsiella pneumoniae* was found to be most susceptible to all the treatments, with Ag/Fe_2O_3 NC as the most active (20 ± 1.16 mm), Ag NPs (18 ± 1.60 mm), and then clove extract (17 ± 1.47 mm). This result emphasizes the better antibacterial activity of the bimetallic nanocomposite. For *Enterobacter cloacae*, there was also the same trend since the nanocomposite proved to be more active (18 ± 1.03 mm) compared to isolated Ag (16 ± 1.13 mm) and Fe_2O_3 NPs (13 ± 1.90 mm). Here, isolated clove extract showed moderate inhibition (15 ± 1.83 mm).

Staphylococcus aureus was clearly the most sensitive strain, especially against Ag NPs (20 ± 1.05 mm) and Ag/Fe_2O_3 NC (21 ± 1.41 mm), which came very close to the level of activity of azithromycin (23 ± 1.07 mm). Clove extract and Fe_2O_3 NPs were also very inhibitory (16 ± 1.80 mm and 14 ± 1.02 mm, respectively). *Bacillus cereus* was more susceptible to the Ag/Fe_2O_3 NC (18 ± 1.18 mm) compared to the free NPs and extract. To our surprise, the nanocomposite was found to be superior to azithromycin (13 ± 1.29 mm) and can be used against drug-resistant bacteria. *Staphylococcus epidermidis* was also susceptible to all nanomaterials, especially the NC (18 ± 1.14 mm) and Ag NPs (17 ± 1.83 mm). The lowest activity was observed with clove extract (11 ± 1.27 mm), whereas the middle level of inhibition was observed with Fe_2O_3 NPs (14 ± 1.26 mm). *Bacillus subtilis* was not inhibited by Ag and Fe_2O_3 NPs but showed a middle-level inhibition by clove extract (14 ± 1.22 mm) and Ag/Fe_2O_3 NC (17 ± 1.26 mm), which reveals that the nanocomposite preserved or strengthened the bioactivity of the extract.

The Ag/Fe_2O_3 nanocomposite showed persistent superior antibacterial effectiveness across tested bacterial strains because silver and iron oxide components function together to improve antimicrobial ability. Ag NPs maintained significant antibacterial properties in a direct action against *Staphylococcus aureus* and *Klebsiella pneumoniae* alongside their established silver-based antibacterial characteristics. The antimicrobial activity of Fe_2O_3 NPs remained inconsistent, but weaker than the activities of Ag NPs and the nanocomposite. The clove extract showed moderate inhibitory actions that validate its position as an antimicrobial phytochemical source while functioning as a nanoparticle synthesis platform. Testing with DMSO revealed no inhibition zone, thus establishing that only the materials used directly affected bacterial growth. These findings demonstrate that green-synthesized nanoparticles, especially Ag/Fe_2O_3 nanocomposites, present significant potential as alternative antibacterial agents to conventional antibiotics for pathogenic bacteria.

The antibacterial activity of the synthesized Ag/Fe_2O_3 nanocomposite in this study, which revealed inhibition zones between 15-21 mm against both Gram-positive and Gram-negative bacteria, is drastically consistent with the reports from the literature. Other similar nanocomposites synthesized using the green approach also displayed significant antibacterial properties caused by the interaction between the silver and iron oxide components. For example, (Al-Zahrani *et al*., 2022 & Al-Zahrani *et al*., 2024) described increased bactericidal activity of Ag/Fe_2O_3 nanocomposites prepared from extracts of buds of *Buddleja lindleyana* and ginger essential oil against *E. coli* and *S. aureus*. (Sihem *et al*., 2020) also established enhanced antibacterial activity of α-Fe_2O_3@Ag nanoparticles synthesized in the presence of *Urtica* leaf extract, implying that Ag doping strongly enhances the efficacy of iron oxide. Further, (Roba *et al*., 2024) stressed on synergistic improvement in the antimicrobial efficiency of Ag/Fe_2O_3 nanocomposites, which correspondence with our results.

Table 3: The results of antibacterial activity against various pathogenic bacteria

Microorganisms	Inhibition zones in mm					
	Clove extract	Ag NPs	Fe_2O_3 NPs	Ag-Fe_2O_3 NC	Control (EtOH, 70%)	Azithromycin
Gram-negative bacteria						
***Escherichia coli* (ATCC 10536)**	14±1.50	17±1.08	13±1.76	15±1.53	NA	17±1.22
***Salmonella typhimurium* (ATCC 25566)**	12±1.26	13±1.09	NA	19±1.57	NA	NA
***Klebsiella pneumonia* (ATCC 10031)**	17±1.47	18±1.60	15±1.17	20±1.16	NA	19±1.09
***Enterobacter cloacae* (DMS 30054)**	15±1.83	16±1.13	13±1.90	18±1.03	NA	NA±1.27
Gram-positive bacteria						
***Bacillus subtilis* (DMS 1088)**	14±1.22	NA	NA	17±1.26	NA	22±1.36
***Bacillus cereus* (EMCC number 1080)**	12±1.31	16±1.30	13±1.17	18±1.18	NA	13±1.29
***Staphylococcus aureus* (ATCC 6538)**	16±1.80	20±1.05	14±1.02	21±1.41	NA	23±1.07
***Staphylococcus epidermidis* (EMCC number 1353[1])**	11±1.27	17±1.83	14±1.26	18±1.14	NA	15±1.33

Results are expressed as mean inhibition zone diameters (mm) ± standard deviation. "NA" indicates no activity or data not available. Ethanol (EtOH, 70%) was used as a negative control, and azithromycin was used as a standard antibiotic (positive control).

Other studies, including those made by (Gao *et al.*, 2013 & Demarchi *et al.*, 2018), also indicated the extraordinary antibacterial activity of the Ag/Fe_2O_3-based nanocomposites and their applicability for long-term and pan-agent antibacterial applications. Heard hitherto, these findings mutually support the efficiency of the Ag/Fe_2O_3 nanocomposite produced in our work and substantiate its attractive role as a green potent antibacterial agent.

Green-synthesized nanoparticles, including Ag NPs and Fe_2O_3 NPs alongside Ag/Fe_2O_3 NC, utilize various combined mechanisms to deteriorate microbial architecture while interrupting their vital biological processes. Ag NPs demonstrate strong antimicrobial activity across many bacterial species. Through releasing Ag^+ ions, nanoparticles activate bacterial cell membranes and enhance their permeability until the cells break down. The cellular function becomes compromised during cellular respiration when these ions attack vital enzymes and proteins through their binding to thiol groups. Ag NPs produce reactive oxygen species, which include superoxide radicals and hydrogen peroxide, that cause DNA damage and harm proteins and lipids while triggering cellular death. Under acidic or bacterial microenvironments, Fe_2O_3 NPs demonstrate peroxidase-like enzyme-mimetic activity that converts H_2O_2 into ROS. Bacterial membranes and biomolecules inside cells become vulnerable to damage through ROS formation. The antimicrobial activities of Fe_2O_3 NPs depend on their ability to induce oxidative stress and interfere with bacterial redox homeostasis, despite being less efficient than Ag NPs.

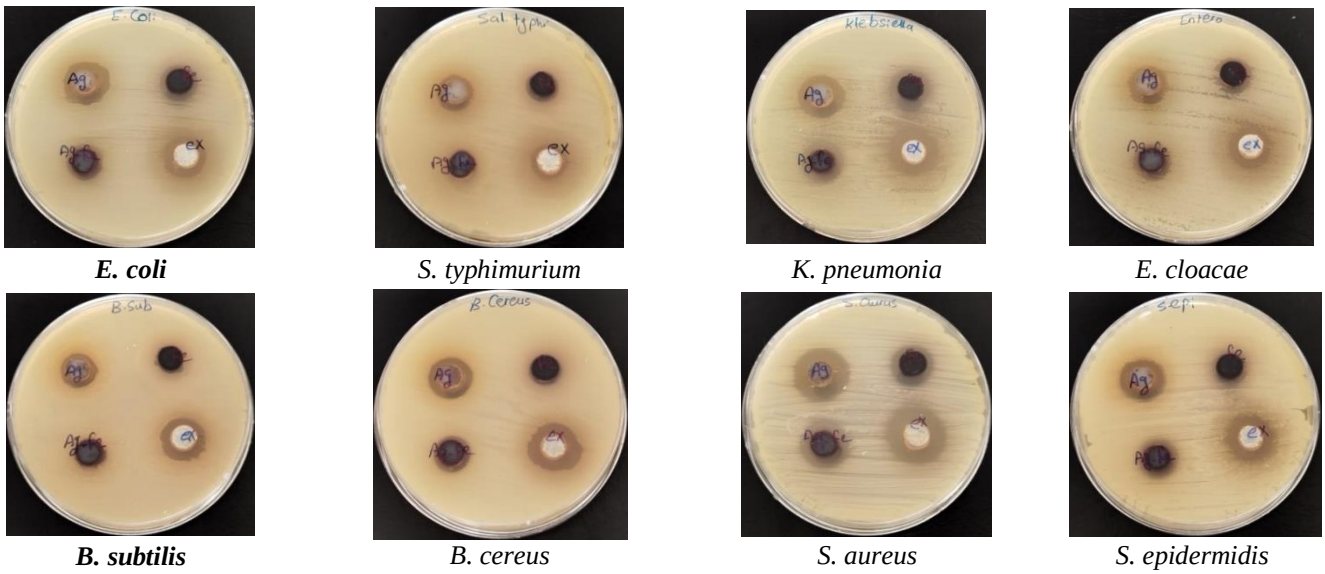

E. coli *S. typhimurium* *K. pneumonia* *E. cloacae*

B. subtilis *B. cereus* *S. aureus* *S. epidermidis*

Figure 8. Photographs of Petri dishes inoculated with bacterial strains, showing the zones of inhibition produced by different treatments. (1) Well containing Clove extract; (2) well containing Ag NPs; (3) well containing Fe_2O_3 NPs; (4) well containing Ag-Fe_2O_3 NC.

The Ag/Fe_2O_3 NC combines the structural features of individual antimicrobial properties of Ag and Fe_2O_3 into a single structure that yields synergistic effects. *S. aromaticum* phytochemicals, eugenol, flavonoids, and tannins stabilize and reduce nanoparticles in green synthesis, enhancing antimicrobial activity in the synthesis. More interactions between contact sites on the nanocomposite surface enhance electrostatic forces to bacterial surfaces and trigger membrane-disruptive effects. The ROS production by both sides of the hybrid arrangement results in a harsh oxidative effect, which is greater than the oxidative effects observed when using single-component nanoparticles.

S. aromaticum phytochemicals from plants, such as eugenol, flavonoids, and tannins, play a role in decreasing and stabilizing the nanoparticles during green synthesis while imparting their own antimicrobial activity. The chemical compounds inhibit microbial enzymes while increasing cellular membrane permeability and causing cell content damage. The nanoparticle surface becomes more accessible and interacts more with bacterial cells because of the phytochemicals. These eco-friendly synthesized nanomaterials destroy bacteria through four mechanisms of action that include compromising the cellular membrane as well as inducing metabolic stress and generating oxidative stress, and inducing degradation of DNA upon being mixed with Ag/Fe_2O_3 nanoparticles, which exhibit maximum antibacterial activity.

CONCLUSION

This study efficiently demonstrated the green synthesis of silver (Ag), iron oxide (Fe_2O_3), and Ag/Fe_2O_3 bimetallic nanoparticles using *Syzygium aromaticum* (clove) extract, a phenolic, flavonoid, and tannin content plant. The phytochemicals not only served as the reducing and stabilizing agents but also imparted powerful biological activities to the resultant nanomaterials. Rigorous characterization using UV-Vis, FTIR, zeta potential, DLS, and HR-TEM ensured efficient formation, stability, and nanoscale morphology of the monometallic and hybrid nanoparticles. Phytochemical content reflected a profound decrease in the content of phenolics, flavonoids, and tannins in nanoparticles derived from crude extract, implying participation of such molecules in capping and the bioreduction process in synthesis. Amongst materials utilized, Ag/Fe_2O_3 NPs were more phytochemicalally abundant compared to monometallic counterparts, implying greater bioactive encapsulation or synergistic stabilizing action. Antioxidant activity, as determined by DPPH• assay, indicated that Ag/Fe_2O_3 NPs possessed an IC_{50} value (0.0098 mg/mL) nearly identical with that of clove extract (0.0097 mg/mL), and greater than traditional ascorbic acid (0.0222 mg/mL). This suggests synergistic improvement of free radical scavenging capability due to the cooperative redox properties of silver and iron oxide and the preserved bioactivity of clove-derived phytochemicals on the nanoparticle surface. Antibacterial activity was found to be robust in Gram-positive and Gram-negative bacterial strains. The Ag/Fe_2O_3 NPs recorded the broadest inhibition zones at all times with a maximum of 21 mm against *S. aureus*, outperforming or matching the standard antibiotic azithromycin in most cases. The activity is enhanced through the synergistic antimicrobial activity of Ag^+ ion release, ROS generation by Fe_2O_3, and enhanced interaction with bacterial membranes due to the combined surface chemistry of the nanocomposite. Briefly, *S. aromaticum* extract offers a cost-effective, environmentally friendly, and biologically active route for green synthesis of multifunctional nanoparticles. The resulting Ag/Fe_2O_3 NPs has exceptional antioxidant and antibacterial properties and holds great promise for biomedical and pharmaceutical uses as antimicrobial coatings, wound healing drugs, and oxidative stress regulators. It should be explored more in the future as its cytotoxicity profile, therapeutic efficacy, and mechanism of action in biological systems to delineate its clinical usefulness.

REFERENCES

Alanazi AA, Saber WI, AlDamen MA and Elattar KM 2024: Green synthesis, characterization, and multifunctional applications of $Ag@CeO_2$ and $Ag@CeO_2$-pullulan nanocomposites for dye degradation, antioxidant, and antifungal activities. *International Journal of Biological Macromolecules*, **280**, p.135862.

Alanazi AA, Saber WI, AlDamen MA and Elattar KM 2025: Sustainable green synthesis of high-performance $Fe_2O_3@CeO_2$-pullulan nanocomposite for efficient dye removal, and antifungal applications. *International Journal of Biological Macromolecules*, **308**, p.142533.

Al-Zahrani FA, AL-Zahrani NA, Al-Ghamdi SN, Lin L, Salem SS and El-Shishtawy RM 2024: Synthesis of Ag/Fe_2O_3 nanocomposite from essential oil of ginger via green method and its bactericidal activity. *Biomass Conversion and Biorefinery*, **14**(12), pp.13265-13273.

Al-Zahrani FA, Salem SS, Al-Ghamdi HA, Nhari LM, Lin L and El-Shishtawy RM 2022: Green synthesis and antibacterial activity of Ag/Fe_2O_3 nanocomposite using Buddleja lindleyana extract. *Bioengineering*, **9**(9), p.452.

Badawy AME, Luxton TP, Silva RG, Scheckel KG, Suidan MT and Tolaymat TM 2010: Impact of environmental conditions (pH, ionic strength, and electrolyte type) on the surface charge and aggregation of silver nanoparticles suspensions. *Environmental science & technology*, **44**(4), pp.1260-1266.

Bamal D, Singh A, Chaudhary G, Kumar M, Singh M, Rani N, Mundlia P and Sehrawat AR 2021: Silver nanoparticles biosynthesis, characterization, antimicrobial activities, applications, cytotoxicity and safety issues: An updated review. *Nanomaterials*, **11**(8), p.2086.

Bayda S, Adeel M, Tuccinardi T, Cordani M and Rizzolio F 2019: The history of nanoscience and nanotechnology: from chemical–physical applications to nanomedicine. *Molecules*, **25**(1), p.112.

Cakić M, Glišić S, Cvetković D, Cvetinov M, Stanojević L, Danilović B and Cakić K 2018: Green synthesis, characterization and antimicrobial activity of silver nanoparticles produced from Fumaria officinalis L. plant extract. *Colloid Journal*, **80**, pp.803-813.

Cartwright A, Jackson K, Morgan C, Anderson A and Britt DW 2020: A review of metal and metal-oxide nanoparticle coating technologies to inhibit agglomeration and increase bioactivity for agricultural applications. *Agronomy*, **10**(7), p.1018.

Demarchi CA, Cruz AB, Sławska-Waniewska A, Nedelko N, Dłużewski P, Kaleta A, Trzciński J, Dal Magro J, Scapinello J and Rodrigues CA 2018: Synthesis of Ag@ Fe2O3 nanocomposite based on O-

carboxymethylchitosan with antimicrobial activity. *International journal of biological macromolecules*, **107**, pp.42-51.

Deshmukh AR, Gupta A and Kim BS 2019: Ultrasound-assisted green synthesis of silver and iron oxide nanoparticles using fenugreek seed extract and their enhanced antibacterial and antioxidant activities. *BioMed research international*, **2019**(1), p.1714358.

Diabate D, N'goran KPDA, Fato TP and Kouassi NGLB 2023: Synthesis of Metallic Silver Supported by Metal Oxides (Fe2O3 and CoO) for the Removal of Methylene Blue in the Presence of Sunlight. *American Journal of Applied Chemistry*, **11**(5), pp.122-129.

Drishya PK, Reddy MV, Mohanakrishna G, Sarkar O, Isha Rohit MV, Patel A and Chang YC 2025: Advances in Microbial and Plant-Based Biopolymers: Synthesis and Applications in Next-Generation Materials. *Macromol*, **5**(2), p.21.

El Badawy AM, Scheckel KG, Suidan M and Tolaymat T 2012: The impact of stabilization mechanism on the aggregation kinetics of silver nanoparticles. *Science of the total environment*, **429**, pp.325-331.

Elattar KM, Al-Otibi FO, El-Hersh MS, Attia AA, Eldadamony NM, Elsayed A, Menaa F and Saber WI 2024a: Multifaceted chemical and bioactive features of $Ag@TiO_2$ and $Ag@SeO_2$ core/shell nanoparticles biosynthesized using *Beta vulgaris* L. extract. *Heliyon*, **10**(7), e28359.

Elattar KM, Ghoniem AA, Al-Askar AA, Bhgat El-Gazzar U, El-Hersh MS, Elsherbiny EA, Eldadamony NM and Saber WI 2024b: Melanin Synthesized by the *Endophytic Aureobasidium* pullulans AKW: A Multifaceted Biomolecule with Antioxidant, Wound Healing, and Selective Anti-Cancer Activity. *Current Topics in Medicinal Chemistry*, **24**(24), pp.2141-2160.

Elattar KM, Ghoniem AA, Al-Otibi FO, El-Hersh MS, Helmy YA and Saber WI 2023: Phytogenic synthesis and characterization of silver metallic/bimetallic nanoparticles using *Beta vulgaris* L. extract and assessments of their potential biological activities. *Applied Sciences*, **13**(18), p.10110.

Elattar KM, Ghoniem AA, Al-Otibi FO, Fakhouri AS, Helmy YA, Saber WI, Hassan MA and Elsayed A 2025: Eco-friendly synthesis of Ag/CeO_2 and CuO/CeO_2 nanocomposites using Curcuma longa extract and assessment of their antioxidant, antifungal, and cytotoxic activities. *RSC Advances*, **15**(16), pp.12100-12116.

Elbagory AM, Rahman A, Cheikhyoussef N, Cheikhyoussef A, Begum NM and Hussein AA 2022: Clove (*Syzygium aromaticum*)-mediated metallic nanoparticles: Synthesis, characterization, and possible pharmacological and industrial applications. In Clove (*Syzygium aromaticum*) (pp. 639-661). Academic Press.

Eldadamony NM, Ghoniem AA, Al-Askar AA, Attia AA, El-Hersh MS, Elattar KM, Alrdahi H and Saber WI 2024: Optimization of pullulan production by Aureobasidium pullulans using semi-solid-state fermentation and artificial neural networks: characterization and antibacterial activity of pullulan impregnated with $Ag-TiO_2$ nanocomposite. *International Journal of Biological Macromolecules*, **269**, p.132109.

El-Khateeb AY, Hesham A, Deyaa A, Salama A, Youssuf A, Ahmed F, Eid M, Saad S, Mohamed S and Rabie MM 2025: From nanotechnology concepts to pioneering patents: Innovations in nanotherapeutic nutrition. *Journal of Agriculture, Food and Environment (JAFE)| ISSN: 2708-5694*, **6**(1), pp.19-38.

El-Maati MFA, Mahgoub SA, Labib SM, Al-Gaby AM and Ramadan MF 2016: Phenolic extracts of clove (*Syzygium aromaticum*) with novel antioxidant and antibacterial activities. *European journal of integrative medicine*, **8**(4), pp.494-504.

El-Saber Batiha G, Alkazmi LM, Wasef LG, Beshbishy AM, Nadwa EH and Rashwan EK 2020: *Syzygium aromaticum* L.(Myrtaceae): traditional uses, bioactive chemical constituents, pharmacological and toxicological activities. *Biomolecules*, **10**(2), p.202.

El-Seedi HR, El-Shabasy RM, Khalifa SA, Saeed A, Shah A, Shah R, Iftikhar FJ, Abdel-Daim MM, Omri A, Hajrahand NH and Sabir JS 2019: Metal nanoparticles fabricated by green chemistry using natural extracts: Biosynthesis, mechanisms, and applications. *RSC advances*, **9**(42), pp.24539-24559.

Gao N, Chen Y and Jiang J 2013: Ag@ Fe2O3-GO nanocomposites prepared by a phase transfer method with long-term antibacterial property. *ACS applied materials & interfaces*, **5**(21), pp.11307-11314.

Ghoniem AA, Elattar KM, Alotaibi AS, Ghabban H, El Hersh MS, El-Khateeb AY, El-Amier YA, El-Gendy HM, Eldadamony NM, Saber WI and Elsayed A 2024: Enhanced resistance of Vigna unguiculata to *Fusarium oxysporum via Rubia cordifolia* extract and growth-promoting endophytic *Bacillus amyloliquefaciens* DW6. *European Journal of Plant Pathology*, **170**(3), pp.567-591.

Ghoniem AA, Elattar KM, Al-Otibi FO, Elsayed A, El-Hersh MS, El-Khateeb AY, Helmy YA and Saber WI 2024: Turmeric extract-mediated biogenic synthesis of $Ag@SeO_2$ magnetic nanoparticles: characterization, optimization, antibacterial and antioxidant activities. *RSC Advances*, **14**(10), pp.7088-7111.

Haiouani K, Hegazy S, Alsaeedi H, Bechelany M and Barhoum A 2024: Green Synthesis of Hexagonal-like ZnO nanoparticles modified with phytochemicals of clove (*Syzygium aromaticum*) and thymus capitatus extracts: enhanced antibacterial, antifungal, and antioxidant activities. *Materials*, **17**(17), p.4340.

Halas NJ, Lal S, Chang WS, Link S and Nordlander P 2011: Plasmons in strongly coupled metallic nanostructures. *Chemical reviews*, **111**(6), pp.3913-3961.

Hammouda MM, Alanazi AA and Elattar KM 2024: Mentha suaveolens Leaves Extract-Mediated Synthesis of $CoO@TiO_2$ and $Fe_2O_3@TiO_2$ Core/Shell Nanoparticles with Synergistic Antimicrobial and Antioxidant Activities. *Chemistry Select*, **9**(17), p.e202401385.

Haro-González JN, Castillo-Herrera GA, Martínez-Velázquez M and Espinosa-Andrews H 2021: Clove essential oil (*Syzygium aromaticum* L. Myrtaceae): Extraction, chemical composition, food applications, and essential bioactivity for human health. *Molecules*, **26**(21), p.6387.

Idris DS and Roy A 2024: Antioxidant and dye degradation activity of green synthesized silver-iron oxide ($Ag-Fe_2O_3$) bimetallic nanoparticles. *Nano-Structures & Nano-Objects*, **38**, p.101142.

Jain K, Takuli A, Gupta TK and Gupta D 2024: Rethinking nanoparticle synthesis: a sustainable approach vs. traditional methods. *Chemistry–An Asian Journal*, **19**(21), p.e202400701.

Jiang HL and Xu Q 2011: Recent progress in synergistic catalysis over heterometallic nanoparticles. *Journal of Materials Chemistry*, **21**(36), pp.13705-13725.

Karaman K and Kaplan M 2022: Composition and functionality of clove (*Syzygium aromaticum*) extracts. In Clove (*Syzygium aromaticum*) (pp. 585-606). Academic Press.

Khurana K and Jaggi N 2021: Localized surface plasmonic properties of Au and Ag nanoparticles for sensors: a review. *Plasmonics*, **16**(4), pp.981-999.

Kumar N and Dixit A 2019: Nanotechnology for defence applications, *Springer International Publishing* (pp. 155-203).

Kumar S, Kumar A, Malhotra T and Verma S 2022: Characterization of structural, optical and photocatalytic properties of silver modified hematite (α-Fe_2O_3) nanocatalyst. *Journal of Alloys and Compounds*, **904**, p.164006.

Kumar S, Kumar M, Velaga S and Singh A 2023: Tuneable optical properties of Fe2O3 magnetic nanoparticles synthesized from Ferritin. *Journal of Sol-Gel Science and Technology*, **105**(3), pp.650-661.

Mahmoud MHH, Ismail AA and Sanad MMS 2012: Developing a cost-effective synthesis of active iron oxide doped titania photocatalysts loaded with palladium, platinum or silver nanoparticles. *Chemical engineering journal*, **187**, pp.96-103.

Mert ME, Mert BD and Elattar KM 2025: Green Synthesis of MoNi@TiO_2 Nanocatalyst for Efficient Methanol Oxidation: Structural, Morphological, and Electrochemical Insights. *Chemistry Select*, *10*(3), p.e202403151.

Mirza AU, Kareem A, Nami SA, Khan MS, Rehman S, Bhat SA, Mohammad A and Nishat N 2018: Biogenic synthesis of iron oxide nanoparticles using Agrewia optiva and Prunus persica phyto species: Characterization, antibacterial and antioxidant activity. *Journal of Photochemistry and Photobiology B: Biology*, **185**, pp.262-274.

Mohan NS, Gokulkumar R, Shankar J, Sridharan R, Logesh B, Sasikumar R, Vallarasu K and Vijayalakshmi V 2022: A facile green approach of Fe2O3, Fe2O3@ Ag, Fe2O3@ AC and Fe_2O_3@ Ag@ AC NPs synthesized via Cocos nucifera L for waste water treatment applications. *Results in Chemistry*, **4**, p.100626.

Naganthran A, Verasoundarapandian G, Khalid FE, Masarudin MJ, Zulkharnain A, Nawawi NM, Karim M, Che Abdullah CA and Ahmad SA 2022: Synthesis, characterization and biomedical application of silver nanoparticles. *Materials*, **15**(2), p.427.

Nandhini G and Shobana MK 2023: Influence of phytochemicals with iron oxide nanoparticles for biomedical applications: a review. *Polymer Bulletin*, **80**(11), pp.11715-11758.

Nishan U, Ullah I, Muhammad N, Afridi S, Asad M, Haq SU, Khan M, Soylak M and Rahim A 2023: Investigation of silver-doped iron oxide nanostructures functionalized with ionic liquid for colorimetric sensing of hydrogen peroxide. *Arabian Journal for Science and Engineering*, **48**(6), pp.7703-7712.

Ogwuegbu MC, Olatunde OC, Pfukwa TM, Mthiyane DM, Fawole OA and Onwudiwe DC 2024: Antibacterial and antifungal activities of *Platycladus orientalis* leaf extract-mediated Fe_2O_3 and Ce-doped Fe_2O_3 nanoparticles. *Discover Applied Sciences*, **6**(10), p.546.

Ovais M, Khalil AT, Islam NU, Ahmad I, Ayaz M, Saravanan M, Shinwari ZK and Mukherjee S 2018: Role of plant phytochemicals and microbial enzymes in biosynthesis of metallic nanoparticles. *Applied microbiology and biotechnology*, **102**, pp.6799-6814.

Padilla-Cruz AL, Garza-Cervantes JA, Vasto-Anzaldo XG, García-Rivas G, León-Buitimea A and Morones-Ramírez JR 2021: Synthesis and design of Ag–Fe bimetallic nanoparticles as antimicrobial synergistic combination therapies against clinically relevant pathogens. *Scientific Reports*, **11**(1), p.5351.

Pandey VK, Srivastava S, Dash KK, Singh R, Dar AH, Singh T, Farooqui A, Shaikh AM and Kovacs B 2024: Bioactive properties of clove (*Syzygium aromaticum*) essential oil nanoemulsion: A comprehensive review. *Heliyon*, **10**(1), e22437.

Park Y, Hong YN, Weyers A, Kim YS and Linhardt RJ 2011: Polysaccharides and phytochemicals: a natural reservoir for the green synthesis of gold and silver nanoparticles. *IET nanobiotechnology*, **5**(3), pp.69-78.

Roba S, Negera D and Abebe B 2024: Ag-Fe_2O_3 nanocomposites for synergistically enhanced antibacterial activity. *Inorganic Chemistry Communications*, **160**, p.112019.

Saeed M, Khan MS, Alagawany M, Farag MR, Alqaisi O, Aqib AI, Qumar M, Siddique F and Ramadan MF 2021: Clove (*Syzygium aromaticum*) and its phytochemicals in ruminant feed: an updated review. Rendiconti lincei. *Scienze fisiche e naturali*, **32**, pp.273-285.

Sánchez-Rangel JC, Benavides J, Heredia JB, Cisneros-Zevallos L and Jacobo-Velázquez DA 2013: The Folin-Ciocalteu assay revisited: improvement of its specificity for total phenolic content determination. *Analytical methods*, **5**(21), pp.5990-5999.

Sandhu ZA, Raza MA, Alqurashi A, Sajid S, Ashraf S, Imtiaz K, Aman F, Alessa AH, Shamsi MB and Latif M 2024: Advances in the optimization of Fe nanoparticles: Unlocking antifungal properties for biomedical applications. *Pharmaceutics*, **16**(5), p.645.

Seyoum A, Asres K and El-Fiky FK 2006: Structure–radical scavenging activity relationships of flavonoids. *Phytochemistry*, **67**(18), pp.2058-2070.

Shah A, Sun H, Qiao Z, Khan MU, Ali N, Gao C, Amir J, Aleena S and Kashif M 2024a: Synthesis of Iron Oxide Nanoparticles and its Antimicrobial, Anticancer, Anti-inflammatory, Wound Healing, and Immunomodulatory Activities-A Review. *Phytopharmacology Research Journal*, **3**(3), pp.1-28.

Shah MP, Bharadvaja N and Kumar L 2024b: Biogenic nanomaterials for environmental sustainability: principles, practices, and opportunities. Springer Nature.

Shahriary M, Veisi H, Hekmati M and Hemmati S 2018: In situ green synthesis of Ag nanoparticles on herbal tea extract (*Stachys lavandulifolia*)-modified magnetic iron oxide nanoparticles as antibacterial agent and their 4-nitrophenol catalytic reduction activity. *Materials Science and Engineering: C*, **90**, pp.57-66.

Sharma C, Ansari S, Ansari MS and Satsangee SP 2022: Phyto-mediated synthesis of Pt and Au/Pt bimetallic nanoparticles using *Syzygium aromaticum* bud-extract: Study of their catalytic, antibacterial, and antioxidant activities. *Journal of Industrial and Engineering Chemistry*, **111**, pp.499-508.

Sharma C, Ansari S, Ansari MS, Satsangee SP and Srivastava MM 2020: Single-step green route synthesis

of Au/Ag bimetallic nanoparticles using clove buds extract: Enhancement in antioxidant bio-efficacy and catalytic activity. *Materials Science and Engineering: C*, **116**, p.111153.

Shraim AM, Ahmed TA, Rahman MM and Hijji YM 2021: Determination of total flavonoid content by aluminum chloride assay: A critical evaluation. *Lwt*, **150**, p.111932.

Shrestha S, Wang B and Dutta P 2020: Nanoparticle processing: Understanding and controlling aggregation. *Advances in colloid and interface science*, **279**, p.102162.

Sihem L, Hanine D and Faiza B 2020: Antibacterial activity of α-Fe_2O_3 and α-Fe_2O_3@ Ag nanoparticles prepared by urtica leaf extract. *Nanotechnologies in Russia*, **15**(2), pp.198-203.

Tantra R, Schulze P and Quincey P 2010: Effect of nanoparticle concentration on zeta-potential measurement results and reproducibility. *Particuology*, **8**(3), pp.279-285.

Vaseghi Z, Nematollahzadeh A and Tavakoli O 2018: Green methods for the synthesis of metal nanoparticles using biogenic reducing agents: a review. *Reviews in Chemical Engineering*, **34**(4), pp.529-559.

Wang YW, Hong BH and Kim KS 2005: Size control of semimetal bismuth nanoparticles and the UV− visible and IR absorption spectra. *The Journal of Physical Chemistry B*, **109**(15), pp.7067-7072.

Ying S, Guan Z, Ofoegbu PC, Clubb P, Rico C, He F and Hong J 2022: Green synthesis of nanoparticles: Current developments and limitations. *Environmental Technology & Innovation*, **26**, p.102336.

Zhang Q, Lee I, Ge J, Zaera F and Yin Y 2010: Surface-Protected Etching of Mesoporous Oxide Shells for the Stabilization of Metal Nanocatalysts. *Advanced Functional Materials*, **20**(14), pp.2201-2214.